



Z-Shaped toroidal dipole planar terahertz metasurfaces

Jianyu Zhu¹ · Shuang Wang¹ · Xiaoli Zhao¹ · Song Wang¹ · Quan Li^{1,2} · Tai Chen¹

Received: 18 October 2019 / Accepted: 9 February 2020 / Published online: 24 February 2020
© Springer-Verlag GmbH Germany, part of Springer Nature 2020

Abstract

We proposed and fabricated a Z-shaped toroidal dipole terahertz metasurfaces, consisting of two incomplete U-shaped split rings, and the two incomplete U-shapes are rotationally symmetric with respect to the Z-axis. The effects of the structural parameters on the electromagnetic characteristics of toroidal resonances are investigated via simulation and experiment. The mechanism of toroidal dipole resonance is studied deeply by establishing an LC resonance model and calculating the multipoles scattering energy. The capacitance was highly depended on the value of lx , and the inductance was determined by the value of ly . Hence, the red shift was observed as the increasing of ly/lx . The resonant frequency of the toroidal dipole resonance is red shifted, as the ly/lx of the metallic pattern increases. The tunability of toroidal dipole resonant frequencies explores the interaction of toroidal multipoles with terahertz wave that could have extensive applications in the terahertz functional devices.

1 Introduction

Terahertz wave is between 0.1 THz and 10 THz, and the wavelength is between 30 and 3000 μm [1]. The natural materials applied in the terahertz band are very rare, which greatly limits the application of terahertz wave [2]. The generation of metamaterials paves a new path for the application of terahertz wave [3–7]. Metamaterials are composite arrays of artificially structured materials, where the dimensions of the unit cell are sufficiently smaller than the wavelength of the incident radiation [8]. We can control the electromagnetic properties of the metamaterials by designing the unit structure. With further research, three-dimensional (3D) metamaterials [2, 9–17] gradually develop to two-dimensional (2D) metasurfaces [8, 18–31] with many virtues,

such as easier to manufacture, smaller thickness and simpler structure.

The toroidal dipole is a member of the multipole family [3], which has the unique electromagnetic properties, such as high quality factor (Q) [10], anisotropy [32], optical rotation [33] and so on. The concept of the toroidal dipole was first proposed by Zel'dovich [34] in 1957. The electromagnetic response of the toroidal dipole in nature is relatively weak, so it is difficult to be detected and studied [2]. Designing proper unit structure of metamaterials/metasurfaces, the toroidal dipole response was enhanced, and the electric and/or magnetic multipole resonances were suppressed. The toroidal dipole metamaterials/metasurfaces were first realized experimental in microwave band, then in optical band, and last in terahertz band [35]. At terahertz frequencies, the toroidal dipole not only has great research value of basic physics, but also has broad application prospects, such as sensors [36], negative index of refraction [37] and dichroism functional devices and so on [38]. In 2017, Cong Longqing et al. [39] proposed a spin induced toroidal dipole in terahertz metasurfaces. Only the power of magnetic field was used to explain the toroidal dipole, and no mathematical model was established to further analyze the toroidal dipole resonance. In 2019, Song Zhengyong et al. [40] designed a tunable toroidal dipole resonance at terahertz band, enabled by a vanadium dioxide metamaterials. The authors studied the toroidal dipole resonance by changing the thickness of SiO_2 and VO_2 , but they had not analyzed

Electronic supplementary material The online version of this article (<https://doi.org/10.1007/s00340-020-7395-5>) contains supplementary material, which is available to authorized users.

✉ Shuang Wang
wangshuang@tute.edu.cn

¹ School of Electronic Engineering, Tianjin University of Technology and Education, Tianjin 300222, China

² National-Local Joint Engineering Laboratory of Intelligent Manufacturing Oriented Automobile Die and Mould, Tianjin University of Technology and Education, Tianjin 300222, China

the mechanism of the toroidal dipole in depth. The power of multipole moment and LC resonance model were not mentioned in the paper. With the combination of terahertz waves and toroidal dipole, scientists believe that the unique characteristics of terahertz waves combined with the singular electromagnetic response characteristics of toroidal dipole will inevitably produce new electromagnetic characteristics and new physical phenomena.

In this paper, we designed and fabricated a metasurfaces that can generate a stable toroidal dipole resonance under the excitation of terahertz waves. The metasurfaces consists of two incomplete U-shaped split rings, and the two incomplete U-shapes are rotationally symmetric with respect to the Z-axis, so the new Z-shaped structure is formed. We studied the mechanism of the toroidal dipole via the change of the metallic pattern parameters, such as the horizontal length of strip (l_x) and the vertical length of strip (l_y), and the surface current and magnetic field distribution were also discussed. To analyze toroidal dipole resonance more in depth, LC resonant circuit model was built, and the multipole scattering energy was calculated. The design of toroidal dipole metasurfaces can achieve a wide range of frequency tuning at terahertz frequencies. Because the toroidal dipole metasurfaces has a wide tuning band and a high transmittance, it can be used in the manufacture of terahertz devices.

2 Metasurfaces sample design and manufacture

Figure 1a shows the unit cell structure of the metasurfaces. The metasurfaces is composed of a substrate layer (silicon) and a metal layer (aluminum). The metallic pattern is composed of two incomplete U-shaped split rings, and the two

U-shapes are rotationally symmetric with respect to the Z-axis, so the Z-shaped metallic patterns were formed. The outer dimensions of the Z-shaped metallic pattern ($l_x \times l_y$) are $90 \mu\text{m} \times 45 \mu\text{m}$, and the width of metal strip (w) is $6 \mu\text{m}$, and the thickness of metallic pattern (t_{hm}) is 200 nm . The substrate is high resistance silicon having a dielectric constant of 11.9 , and the thickness of the substrate (t) is $640 \mu\text{m}$. To study the electromagnetic characteristics more in depth, we set the parameters l_y ($l_y = 30 \mu\text{m}, 35 \mu\text{m}, 40 \mu\text{m}$ and $45 \mu\text{m}$) and l_x ($l_x = 60 \mu\text{m}, 70 \mu\text{m}, 80 \mu\text{m}$ and $90 \mu\text{m}$), then the corresponding samples were fabricated.

The dimensions of metasurfaces were in the micrometers; hence photolithography and metallization manufacturing processes were employed to manufacture metasurfaces samples. Firstly, the photoresist was coated on a piece of clean silicon wafer followed by patterning with the proper mask. Secondly, 200 nm thick aluminum film was deposited on the patterned photoresist using vacuum coating equipment. Finally, aluminum deposited wafers were soaked in acetone for lift-off to get the metasurfaces samples [8, 26]. Figure 1b shows microscope image of the fabricated sample with $l_x = 70 \mu\text{m}$ and $l_y = 40 \mu\text{m}$. The electromagnetic characteristics of samples were measured via 8F terahertz time-domain spectroscopy (THz-TDS) [41].

3 Results and discussion

Figure 2 shows the experimental and simulated transmission spectrum of metasurfaces with different l_y and l_x . The frequencies and transmitted intensity of toroidal dipole resonance are changed with the variation of metallic patterns parameters. As shown in Fig. 2a, the resonant frequency decreases from 0.62988 THz to 0.46875 THz

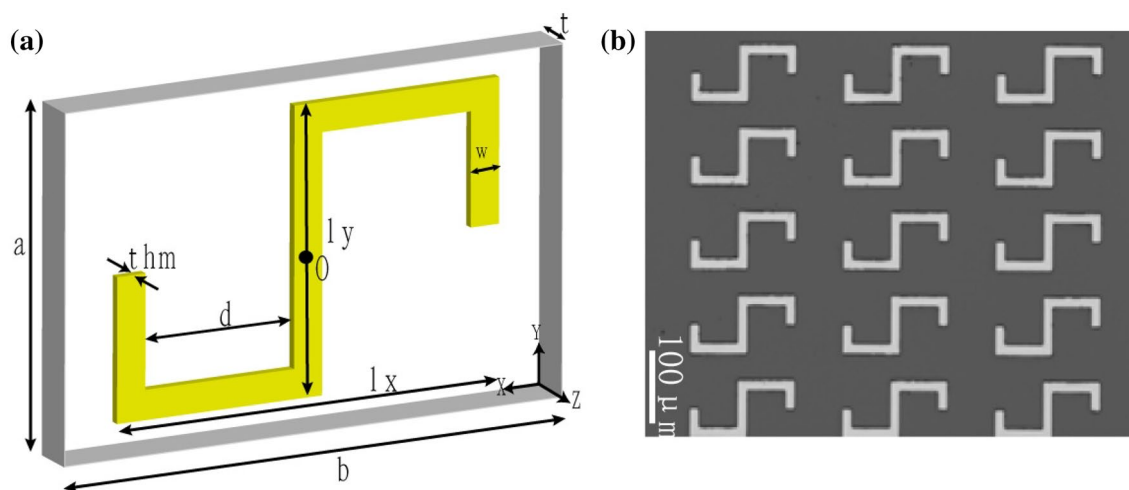
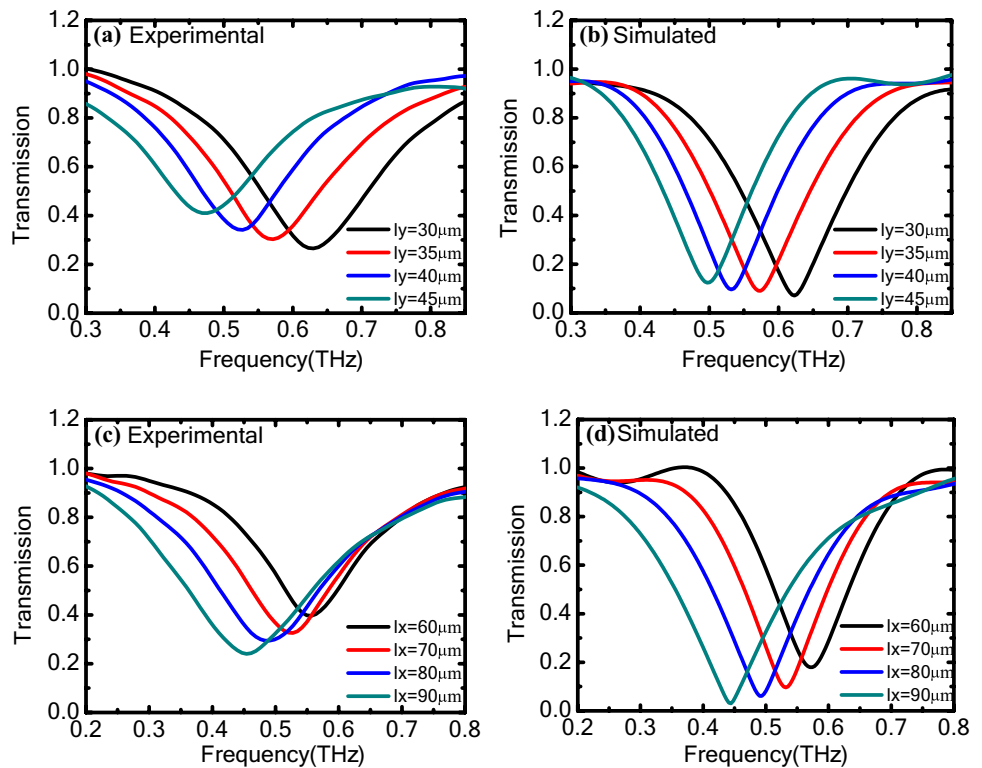


Fig. 1 a Schematic of the proposed metasurfaces metamolecule. b Microscope image of the fabricated sample with $l_x = 70 \mu\text{m}$ and $l_y = 40 \mu\text{m}$

Fig. 2 Experimental (a, c) and simulated (b, d) amplitude transmission spectra for samples with different values of ly and lx



as the value of ly increases, and a red shift is observed. The transmitted intensity increases from 0.2651 to 0.4103. When the value of ly is 45 μm , the variation of the toroidal dipole resonant frequency reaches maximum value (0.16113 THz), and the transmission intensity decreases by 0.1452. Figure 2c shows that the frequency of the toroidal dipole resonance is red-shifted as the value of lx increases in the measured transmission. As the increase of lx , the resonance frequency is changed from 0.5566 THz to 0.4541 THz, and the transmitted intensity is changed from 0.3965 to 0.2403. When the value of lx is 90 μm , the frequency variation of the toroidal dipole resonance reaches maximum value (0.1025 THz); however, the transmission intensity increases by 0.1562. The frequency and the transmitted intensity of the toroidal dipole resonance can be tuned by the variation of ly or lx .

Figure 2b and d show the simulated transmission of the metasurfaces as ly or lx increase, respectively. The metasurfaces parameters of aluminum are described by the Drude model, where the angular frequency dependent permittivity is given by $\epsilon(\omega) = \epsilon_\infty - \left[\frac{\omega_p^2}{\omega(\omega + i\Gamma)} \right]$, with the plasma frequency ω_p set as $22.43 \times 10^{15} \text{ rad s}^{-1}$ and the damping rate $\Gamma = 124.34 \times 10^{12} \text{ rad s}^{-1}$ [8, 42]. By comparison of experimental and simulated results, we found that the simulated and experimental transmission of the metasurfaces is very similar, although there are some differences in the transmitted intensity and resonant

frequencies. The certain differences were due to due to the inevitable fabricating, machining and measurement deviations.

In simulation, we observed the surface current distribution and the magnetic field distribution, as shown in Fig. 3. Only one surface current distribution figure is demonstrated in Fig. 3a, because the surface currents distribution of the metasurfaces is almost the same with different ly/lx . The two current loops of the metasurfaces are flowing along two directions on the XY plane at $Z=0$, which were indicated by the black arrow on the XY plane. The surface current formed a loop along incomplete U-shape split ring, which was the typical LC-induced resonance. The current loop on the left is anticlockwise, and the current loop on the right is clockwise, hence their magnetic dipole moment pointed in the opposite direction along the Z-axis according to the right hand rule. The toroidal dipole was formed accordingly, which is labeled by the blue circle. As shown in Fig. 3b–i, the induced magnetic field distribution is arranged head-to-tail, which are typical characteristics of toroidal dipole resonance [43]. As shown in Fig. 3b–e, the intensity of toroidal dipole was slightly weakened as the ly increasing. Figure 3f–i show the intensity of toroidal dipole was weakened as the lx increasing.

To analyze the relation between resonance frequency and the structural parameters of toroidal dipole metasurfaces deeply, we built a LC resonant model for the metasurfaces, and effective circuit was shown in Fig. 4. The

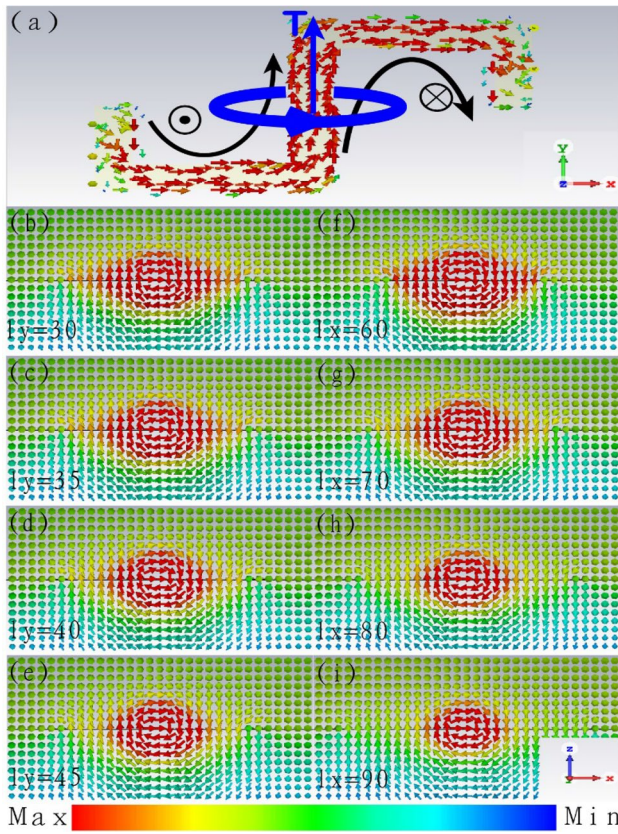


Fig. 3 (a) Schematics of the formation of toroidal dipole resonance, **b–e** magnetic field distribution with $l_y = 30 \mu\text{m}$, $35 \mu\text{m}$, $40 \mu\text{m}$ and $45 \mu\text{m}$ (on the XZ plane at $Y=0$), **f–i** magnetic field distribution with $l_x = 60 \mu\text{m}$, $70 \mu\text{m}$, $80 \mu\text{m}$ and $90 \mu\text{m}$ (on the XZ plane at $Y=0$)

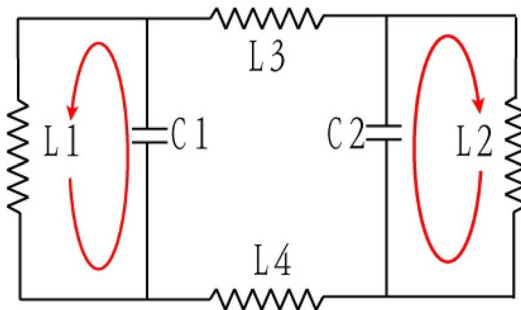


Fig. 4 LC resonant circuit

two rotational symmetric incomplete U-shape split ring resonators provided inductance $L1$ and $L2$, and the coupling between two adjacent incomplete U-shape split ring resonators provided the inductance $L3$ and $L4$. The split gap between short arms and long arms provided capacitors $C1$ and $C2$. According to the LC resonance model, the total capacitance of metasurfaces (C) was set as $C = C1 + C2$, and the total inductance of metasurfaces (L) was set as $L = L1 + L2 + L3 + L4$. Capacitance, inductance

Table 1 Calculated, experimental and simulated toroidal dipole resonant frequencies as l_y and l_x increasing

l_y (μm)	30	35	40	45
Calculated frequency (THz)	0.6636	0.5871	0.5321	0.4901
Experimental frequency (THz)	0.6299	0.5713	0.5273	0.4688
Simulated frequency (THz)	0.623	0.572	0.532	0.497
l_x (μm)	60	70	80	90
Calculated frequency (THz)	0.5579	0.5321	0.5084	0.4869
Experimental frequency (THz)	0.5566	0.5273	0.4907	0.4541
Simulated frequency (THz)	0.571	0.532	0.493	0.4445

Table 2 Capacitance and inductance values with different l_x

l_x (μm)	60	70	80	90
C (F)	2.09×10^{-29}	1.69×10^{-29}	1.41×10^{-29}	1.22×10^{-29}
L (H)	4.02×10^{-9}	4.69×10^{-9}	5.36×10^{-9}	6.03×10^{-9}

and resonant frequencies (f) would be explained by the formula as following [17, 44]:

$$C = \frac{\epsilon \cdot \text{thm} \cdot \left(\frac{l_y}{2} - w\right)}{2\pi kd} \tag{1}$$

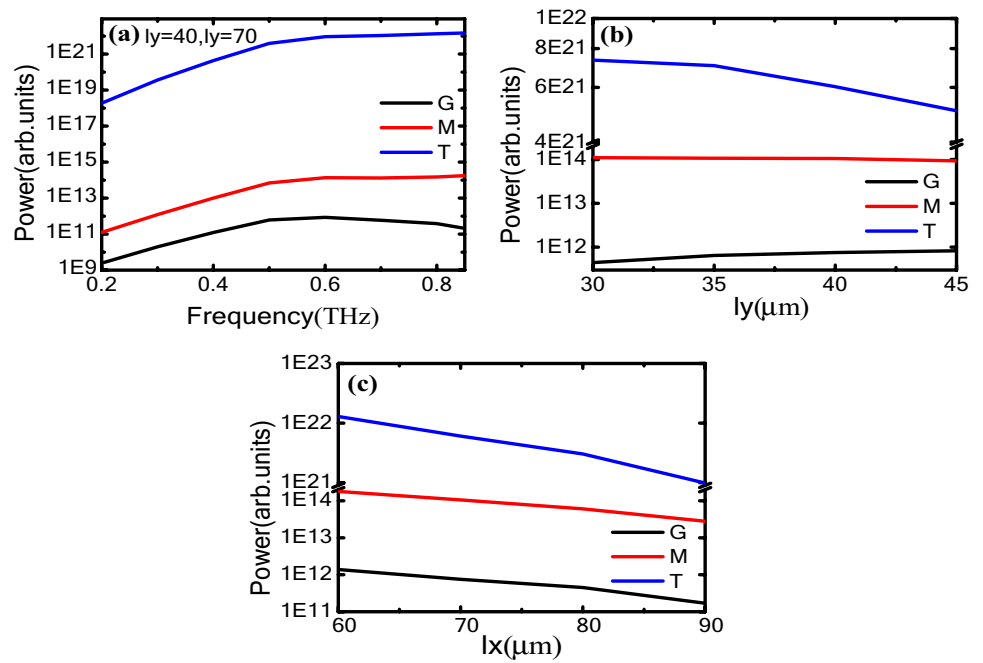
$$L = \frac{\mu_0 t \cdot l_x}{2w} \tag{2}$$

$$f = \frac{c}{2\pi\sqrt{LC}} \tag{3}$$

where, $\epsilon = \epsilon_0\epsilon_r$ is the permittivity of the dielectric in the split gap of the metallic pattern; k is the electrostatic force constant; μ_0 is the permeability of vacuum; l_y is the vertical length of strip; l_x is the horizontal length of strip; thm is the thickness of the metal on the metasurfaces; d is the distance between the long metal arm and the short metal arm of the metallic pattern; t is the thickness of the silicon wafer; c is a variable related to l_x , as shown in Fig. 1.

According to the formulas (1), (2) and (3), we could calculate the corresponding frequency value with the variation of l_y and l_x , as shown in Table 1. The calculated resonant frequency is very similar to the experimental and simulated values, and the maximum error is no more than 0.05 THz. According to the formulas (1) and (3), C is increased as l_y increases, so frequency is decreased. According to formulas (1), (2) and (3), when d increases as l_x increasing, C is decreased and L is increased. According to the formulas (1) and (2), the calculated values of L and C are listed in Table 2. We found that the variation of

Fig. 5 **a** Dispersion of scattering power for various multipole moments induced in the toroidal metasurfaces. Dispersion of scattering power for various multipole moments induced in the toroidal metasurfaces **b** with different ly and **(c)** with different lx



L is much larger than the variation of C as lx is increased, so inductance plays a major role for the influence of frequency. This explains why the toroidal dipole resonance is red-shifted as ly and lx increased. In summary, the LC resonant model can explain the variation of the toroidal dipole resonance well.

To further illustrate the toroidal dipole phenomenon in metasurfaces, we calculated the scattering energy of the multipoles via the multipole scattering theory according to the volume current density distribution [8, 45, 46]. However, because some multipoles had relatively small energy, only the electric toroidal dipole along X -axis (G), magnetic dipole along Z -axis (M) and toroidal dipole along Y -axis (T) were calculated. The specific G , M and T calculations have the following equations:

Electric dipole (P):

$$P = \frac{1}{i\omega} \int j d^3 r \tag{4}$$

Magnetic dipole (M):

$$M = \frac{1}{2c} \int (r \times j) d^3 r \tag{5}$$

Electric toroidal dipole (G):

$$G = \frac{1}{2} \int (r \times p) d^3 r \tag{6}$$

Toroidal dipole (T):

$$T = \frac{1}{10c} \int [(r \cdot j)r - 2r^2 j] d^3 r \tag{7}$$

where r is the coordinate vector with its origin placed at the center of torus, c is the speed of light, and j is the current density. The simulated current density (j) was obtained via CST Microwave Studio simulations, which are used to calculate the strength of toroidal dipole by means of MATLAB programs.

Figure 5a shows the curve of G , M and T changing with frequency when $ly=40 \mu\text{m}$ and $lx=70 \mu\text{m}$. By comparing G , M , and T , we found that the intensity of T is much greater than G and M at the resonant frequency. As shown in Fig. 5b, the intensity of T is much stronger than that of M and G , so the toroidal dipole resonance dominates the resonant frequencies. The intensity of T is decreased as the ly increasing, which is coincidence with the magnetic field distribution shown in Fig. 3b–e. Figure 5c shows the intensity of T is much stronger than that of M and G , so the toroidal dipole resonance dominates the resonant frequencies. The intensity of T is decreased as the lx increasing, which is coincidence with the magnetic field distribution shown in Fig. 3f–i.

4 Conclusion

We designed Z-shaped toroidal dipole metasurfaces in the terahertz band. The toroidal dipole was studied by changing the ly and lx parameters via simulation and experiment. We

found that the electromagnetic characteristics of the toroidal dipole could be tuned by ly and lx . To better understand the toroidal dipole resonance, we established the LC resonance model and obtained the mathematical capacitance and inductance formula with the independent variables ly and lx . The red shift phenomena were well explained by the LC resonance model, which helped us to understand the mechanism of toroidal dipole resonance deeply. We calculated T , M and G to further illustrate the toroidal dipole phenomenon. The toroidal dipole resonances dominated at the resonant frequencies. The variation of T had the same tendency as the magnetic field distribution. Therefore, the electromagnetic characteristics of toroidal dipole metasurfaces would be tuned by the changing of structural parameters, which have potential to develop more terahertz functional devices.

Acknowledgement This research was supported by the National Natural Science Foundation of China (Grant numbers 61505146 and 61705167), and the Science Development Foundation of Tianjin University of Technology and Education (Grant number KJ1920), and the Start-up project of scientific research of Tianjin University of Technology and Education (Grant number KYQD1718 and KYQD1907).

References

- Z. Yan, Y. Ying, H. Zhang, H. Yu, Proc. SPIE Int. Soc. Opt. Eng. **6373**, 6373OR (6373OR)
- Y. Bao, X. Zhe, Z. Fang, Sci. Rep. **5**, 11793 (2015)
- J. Gu, R. Singh, Z. Tian, W. Cao, Q. Xing, M. He, J.W. Zhang, J. Han, H.T. Chen, W. Zhang, Appl. Phys. Lett. **97**, 071102 (2010)
- H.T. Chen, W.J. Padilla, J.M.O. Zide, A.C. Gossard, A.J. Taylor, R.D. Averitt, Nature **444**, 597 (2006)
- W.M. Zhu, A.Q. Liu, X.M. Zhang, D.P. Tsai, Adv. Mater. **23**, 1792 (2011)
- X. Zhang, Z. Tian, W. Yue, J. Gu, S. Zhang, J. Han, W. Zhang, Adv. Mater. **25**, 4567 (2013)
- X. Zhang, S. Yang, W. Yue, Q. Xu, C. Tian, X. Zhang, E. Plum, S. Zhang, J. Han, W. Zhang, Optica **6**, 1190 (2019)
- M. Gupta, N. Savinov, L. Xu, C. Cong, S. Dayal, Adv. Mater. **28**, 8206 (2016)
- C.M. Soukoulis, M. Wegener, Nat. Photonics **5**, 523 (2011)
- Z. Liu, S. Du, A. Cui, Z. Li, Y. Fan, S. Chen, W. Li, J. Li, C. Gu, Adv. Mater. **29**, 1606298 (2017)
- A.A. Basharin, M. Kafesaki, E.N. Economou, C.M. Soukoulis, Phys. Rev. X **5**, 011036 (2014)
- V. Yannopapas, A.G. Vanakaras, ACS Photonics **2**, 1030 (2015)
- H. Xiang, L. Ge, L. Liu, T. Jiang, Z.Q. Zhang, C.T. Chan, D. Ham, Phys. Rev. B **95**(6), 045403 (2016)
- S.L. Wang, J.J. Xiao, Q. Zhang, X.M. Zhang, Opt. Express **22**, 24358 (2014)
- W. Liu, J. Zhang, B. Lei, H. Hu, A.E. Miroshnichenko, Opt. Lett. **40**(11), 113105 (2015)
- S.H. Kim, S.S. Oh, K.J. Kim, J.E. Kim, H.Y. Park, O. Hess, C.S. Kee, Phys. Rev. B **91**, 035116 (2015)
- W.X. Lim, S. Han, M. Gupta, K.F. Macdonald, R. Singh, Appl. Phys. Lett. **111**(6), 061104 (2017)
- M. Gupta, Y.K. Srivastava, M. Manjappa, R. Singh, Appl. Phys. Lett. **110**(12), 121108 (2017)
- L. Cong, Y.K. Srivastava, R. Singh, Appl. Phys. Lett. **111**(8), 081108 (2017)
- S. Han, M. Gupta, L. Cong, Y.K. Srivastava, R. Singh, J. Appl. Phys. **122**(11), 113105 (2017)
- T.C.W. Tan, E. Plum, R. Singh, Photonics **6**(3), 75 (2019)
- Y.K. Srivastava, R.T. Ako, M. Gupta, M. Bhaskaran, S. Sriram, R. Singh, Appl. Phys. Lett. **115**, 151105 (2019)
- Q. Li, L. Cong, R. Singh, N. Xu, W. Cao, X. Zhang, Z. Tian, L. Du, J. Han, W. Zhang, Nanoscale **8**, 17278 (2016)
- Y. Fan, T. Qiao, F. Zhang, Q. Fu, J. Dong, B. Kong, H. Li, Sci. Rep. **7**, 40441 (2017)
- M. Manjappa, Y.K. Srivastava, R. Singh, Phys. Rev. B **94**, 161103(R) (2016)
- R. Yahiaoui, J.A. Burrow, S.M. Mekonen, A. Sarangan, J. Mathews, I. Agha, T.A. Searles, Phys. Rev. B **97**, 155403 (2017)
- J.A. Burrow, Y. Riad, S. Andrew, I. Agha, J. Mathews, T.A. Searles, Opt. Express **25**, 32540 (2017)
- M. Papaioannou, E. Plum, J. Valente, E.T. Rogers, N.I. Zheludev, Light Sci. Appl. **5**, e16070 (2016)
- L. Cong, V. Savinov, Y.K. Srivastava, S. Han, R. Singh, Adv. Mater. **30**, 1804210 (2018)
- M. Gupta, Y.K. Srivastava, M. Manjappa, R. Singh, Appl. Phys. Lett. **110**, 121108 (2017)
- M. Gupta, R. Singh, Adv. Opt. Mater. **4**, 2119 (2016)
- K. Sawada, N. Nagaosa, Phys. Rev. Lett. **95**, 237402 (2005)
- N. Papasimakis, V.A. Fedotov, K.B. Marinov, N.I. Zheludev, Phys. Rev. Lett. **103**, 093901 (2009)
- I.B. Zel'Dovich, J. Exp. Theor. Phys. **6**, 1184 (1958)
- S. Wang, S. Wang, Q. Li, X. Zhao, J. Zhu, Materials **11**, 2036 (2018)
- V. Savinov, V.A. Fedotov, N.I. Zheludev, Phys. Rev. B **89**, 205112 (2014)
- K.B. Marinov, A.D. Boardman, V.A. Fedotov, N.I. Zheludev, New J. Phys. **9**, 324 (2007)
- K. Baryshnikova, D. Smirnova, B. Luk'Yanchuk, Y. Kivshar, Adv. Opt. Mater. **7**, 1801350 (2019)
- L. Cong, R. Singh, Y.K. Srivastava, Conf. Lasers Electro. Opt. (CLEO) **37**, JTu5A (2017)
- Z. Song, Y. Deng, Y. Zhou, Z. Liu, IEEE Photonics J. **11**, 1 (2019)
- D. Grischkowsky, J. Opt. Soc. B **7**, 2006 (1990)
- M.A. Ordal, L.L. Long, R.J. Bell, S.E. Bell, R.R. Bell, R.W. Alexander Jr., C.A. Ward, Appl. Opt. **22**, 1099 (1983)
- A. Ahmadvand, B. Gerislioglu, A. Tomitaka, P. Manickam, A. Kaushik, S. Bhansali, M. Nair, N. Pala, Biomed. Opt. Express **9**, 373 (2018)
- J. Zhou, E.N. Economou, T. Koschny, C.M. Soukoulis, Opt. Lett. **31**, 3620 (2006)
- Z.G. Dong, J. Zhu, J. Rho, J.Q. Li, C. Lu, X. Yin, X. Zhang, Appl. Phys. Lett. **101**, 144105 (2012)
- Y.W. Huang, W.T. Chen, P.C. Wu, V. Fedotov, V. Savinov, Y.Z. Ho, Y.F. Chau, N.I. Zheludev, D.P. Tsai, Opt. Express **20**, 1760 (2012)

Publisher's Note Springer Nature remains neutral with regard to jurisdictional claims in published maps and institutional affiliations.